

Retraction

Retracted: Virtual Reality-Assisted Percutaneous Transluminal Angioplasty for Interventional Treatment of Lower-Extremity Arteriosclerosis Obliterans

Journal of Healthcare Engineering

Received 10 October 2023; Accepted 10 October 2023; Published 11 October 2023

Copyright © 2023 Journal of Healthcare Engineering. This is an open access article distributed under the Creative Commons Attribution License, which permits unrestricted use, distribution, and reproduction in any medium, provided the original work is properly cited.

This article has been retracted by Hindawi following an investigation undertaken by the publisher [1]. This investigation has uncovered evidence of one or more of the following indicators of systematic manipulation of the publication process:

- (1) Discrepancies in scope
- (2) Discrepancies in the description of the research reported
- (3) Discrepancies between the availability of data and the research described
- (4) Inappropriate citations
- (5) Incoherent, meaningless and/or irrelevant content included in the article
- (6) Peer-review manipulation

The presence of these indicators undermines our confidence in the integrity of the article's content and we cannot, therefore, vouch for its reliability. Please note that this notice is intended solely to alert readers that the content of this article is unreliable. We have not investigated whether authors were aware of or involved in the systematic manipulation of the publication process.

Wiley and Hindawi regrets that the usual quality checks did not identify these issues before publication and have since put additional measures in place to safeguard research integrity.

We wish to credit our own Research Integrity and Research Publishing teams and anonymous and named external researchers and research integrity experts for contributing to this investigation.

The corresponding author, as the representative of all authors, has been given the opportunity to register their agreement or disagreement to this retraction. We have kept a record of any response received.

References

- [1] R. Zhou, H. Zhai, Z. Yin, J. Cui, and N. Hu, "Virtual Reality-Assisted Percutaneous Transluminal Angioplasty for Interventional Treatment of Lower-Extremity Arteriosclerosis Obliterans," *Journal of Healthcare Engineering*, vol. 2021, Article ID 9975583, 13 pages, 2021.

Research Article

Virtual Reality-Assisted Percutaneous Transluminal Angioplasty for Interventional Treatment of Lower-Extremity Arteriosclerosis Obliterans

Ruhang Zhou ¹, Hongyan Zhai,² Zhiming Yin,¹ Jian Cui ¹ and Nan Hu ³

¹Department of Vascular Surgery, Bozhou Hospital Affiliated to Anhui University of Science and Technology, QiaoCheng District, Bozhou, Anhui, China

²Department of Ophthalmology, Bozhou Hospital Affiliated to Anhui University of Science and Technology, QiaoCheng District, Bozhou, Anhui, China

³Department of Vascular Surgery, The Affiliated Nanjing Drum Tower Hospital, Nanjing University Medical School, Nanjing City 210000, China

Correspondence should be addressed to Jian Cui; mmyycc@163.com and Nan Hu; 364819080@qq.com

Received 18 March 2021; Revised 12 June 2021; Accepted 17 June 2021; Published 27 July 2021

Academic Editor: Zhihan Lv

Copyright © 2021 Ruhang Zhou et al. This is an open access article distributed under the Creative Commons Attribution License, which permits unrestricted use, distribution, and reproduction in any medium, provided the original work is properly cited.

This study was to evaluate the biomechanical characteristics of the vascular wall during virtual reality- (VR-) assisted percutaneous transluminal angioplasty (PTA) and its effect on the treatment of lower-extremity arteriosclerosis obliterans (LEAO). In this study, a three-dimensional (3D) model and a finite-element model of arteries were constructed first, and various fluid mechanics were analyzed. Then, the virtual expansion simulation (VES) of individualized PTA was performed based on the ABAQUS/Explicit module to analyze the interaction between the balloon and the blood vessel at different times and the changes in the vascular shape and structural stress distribution. Finally, an LEAO animal model was constructed. Based on conventional PTA (PTA group) and VR-assisted PTA (VR-PTA) treatment, the morphological changes of vascular lumen of the two animal models were evaluated. The results showed that the normal, stenotic blood vessels and blood models were successfully constructed; the pressure of the stenotic blood vessel at the stenosis decreased obviously and the shear stress of blood vessel wall increased compared with that of the normal blood vessels, and there may be a blood reflux area in the poststenosis stage. The simulation results of the VES showed that the maximum principal stress value at 3 mm of the marginal vessel was much lower than that at 5 mm (about 10% lower), so the maximum principal stress change within 2 mm of the balloon-expanded vessel was the most obvious. The treatment results of the animal model showed that the VR-PTA group showed an obvious increase in the diameter of the vascular lumen, a decrease in the intima and media area, and a decrease in the thickness of the vessel wall in contrast to the PTA group ($P < 0.05$), which had an important effect on the reconstruction and expansion of the vascular lumen. The VR-PTA treatment on LEAO was realized in this study, which provided critical reference for the follow-up application of VR technology in the evaluation of surgical plan and research on biomechanical mechanisms of restenosis after PTA.

1. Introduction

Atherosclerosis obliterans is one of the ischemic diseases with the highest incidence, and its prevalence is increasing year by year. The main manifestation of the disease is arteriosclerosis occlusion of the lower extremities, of which 30% occur in the iliac artery, and the other 70% are more common in the femoral artery, popliteal artery, and distal artery [1]. The clinical manifestations of arteriosclerosis

occlusion of the lower extremities often show intermittent claudication, resting pain, and gangrene; and the severe progress of which may even affect the life safety of the patient [2]. Atherosclerosis is the main cause of arteriosclerosis and occlusion. A large number of studies have shown that physiological processes such as vascular endothelial dysfunction, body inflammation, and endothelial cell apoptosis are closely related to the occurrence and development of atherosclerosis [3]. In addition, studies have confirmed that

atherosclerosis occurs mostly in the complex flow area of blood vessels. For example, arterial bifurcation, bending, and local stenosis are all important factors that trigger complex flow of blood vessels. Therefore, atherosclerosis is prone to causing blood vessel block [4, 5].

PTA uses an inflation balloon to expand at the vascular stenosis to relieve the vascular stenosis, which can reduce the damage caused by the stent coating to the diseased blood vessel [6]. It is mainly to treat complex lesions such as tortuous, diffuse, and severe stenosis, but the interaction between the balloon and the blood vessel can easily cause damage to the blood vessel wall [7]. Finite element is a numerical calculation method for structural analysis, and it has been widely used in the field of biomechanics. At present, the finite-element method has been applied to simulate the virtual simulation of the stent placement process, and conduct a preliminary assessment of the vascular damage caused during the process [8, 9]. As PTA is prone to tearing of the vascular intima, and postoperative plaque prolapse, elastic retraction of the vessel walls, and vascular remodeling, it is easy to cause acute occlusion and restenosis of blood tubes, which largely limits its clinical application [10]. Both stent placement and bypass vessel grafting have higher surgical risks and higher surgical costs. Therefore, accurate assessment of the biomechanics of the blood vessel wall and blood flow during PTA treatment is of great significance for improving the prognosis of patients.

In this study, a 3D model and a finite-element model of blood vessels were firstly constructed to analyze the characteristics of normal blood vessels and stenotic blood vessels. The ABAQUS/Explicit software was adopted to perform VES of PTA to simulate the interaction between the balloon and the blood vessel at different times and analyze the changes in the vascular shape and structural stress distribution. The LEAO animal model was constructed, and conventional PTA and VR-assisted PTA treatment were performed respectively, and the effects of different methods on the morphology of the stenotic vessels of the model were compared. This study aimed to provide new reference for the treatment of atherosclerosis.

2. Experimental Methods

2.1. Construction of an Individualized 3D Model of Blood Vessels. According to the data of computed tomography angiography (CTA), the multi-planar reconstruction technology was used to construct the individualized 3D structure model of the blood vessel. The interactive medical modeling and simulation software Mimics17.0 was applied to construct the inner surface of the blood vessel wall. The software package contained an artery segmentation module, which could realize the segmentation and reconstruction of the inner surface of the artery. The starting position of the aorta was selected and determined, and the end point of the blood vessel of interest was determined. After the parameters were set according to the requirements, the arterial lumen data could be automatically generated. The files generated by Mimics17.0 software were imported into Geomagic Studio 12.0 software to optimize the model. The mixed and noise data were processed first using the point cloud technology; the Polygon phase software was adopted to generate triangles under polygon processing (hole filling, smooth filling, and surface smoothing) to obtain a solid model; and the generated model was exported back to the Mimics17.0 software. Due to the unevenness of the thickness of the blood vessel wall after arteriosclerosis (as shown in Figure 1), plaque and vascular remodeling all exacerbated the difference in the thickness of diseased and nonpathological blood vessels.

It can only distinguish between soft plaques and calcified plaques but cannot quantitatively analyze the material properties of the blood vessel wall using the CTA technology. The patients with LEAO considered in this study were soft plaque lesions, so they were defined as a single vascular wall material property. According to the isotropic hyperelastic constitutive relationship constructed by Holzapfel et al. [11] to characterize the properties of coronary artery wall materials, the sixth-order reduced polynomial strain energy constitutive model was adopted to calculate its density function, and the mathematical expression was expressed as follows:

$$I = C_{10}(\bar{A}_1 - 3) + C_{20}(\bar{A}_1 - 3)^2 + C_{30}(\bar{A}_1 - 3)^3 + C_{40}(\bar{A}_1 - 3)^4 + C_{50}(\bar{A}_1 - 3)^5 + C_{60}(\bar{A}_1 - 3)^6, \quad (1)$$

In equation (1), \bar{A}_1 was the first invariant in the Cauchy–Green tensor. Affected by the blood vessel density ($1.12 \times 10^{-3} \text{ g mm}^{-3}$), the value of C_{i0} was 6.52×10^{-3} , 4.89×10^{-3} , 9.62×10^{-3} , 7.60×10^{-3} , -4.30×10^{-3} , and 8.69×10^{-3} , respectively.

2.2. Construction of the Finite-Element Model. Then, the CAE modeling tool in the ANSYS software was adopted to mesh the vessel wall. Based on the dependence of the mesh, the element type was set to hexahedron C3D8R, with the maximum size of 0.0075 mm, the number of meshes of 400,000, the number of nodes of 500,000, the elasticity modulus of 0.6 MPa, and the Poisson's ratio of 0.45. The size

of each grid cell showed an exponential decrease from the outside to the inside, based on which a discretized grid model of blood vessels was constructed.

The blood was set as the fluid domain for analysis only, and the blood inlet, outlet, and coupling face were set, respectively. The fluid domain belonged to the computational domain of the field of fluid mechanics. In the calculation of finite-element fluid mechanics, differential equations could be used to realize the conversion of Gauss equation to integral equation. Larger diameter arteries were more suitable for fluid dynamics models. If the diameter of the blood vessel was larger than 0.5 mm, the flow shear rate of blood was higher. The viscosity of blood could be regarded as a

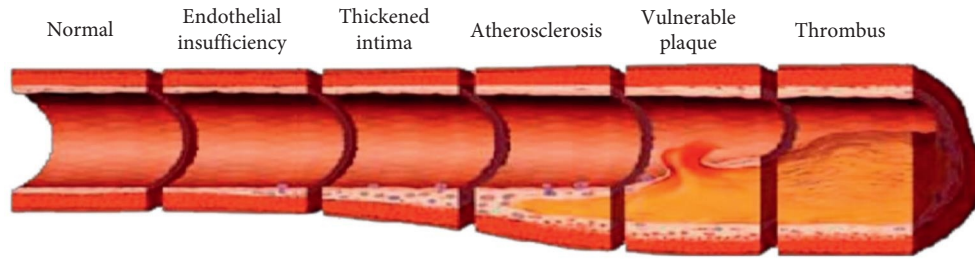


FIGURE 1: Schematic diagram of arteriosclerosis formation.

constant, and blood was a viscous Newtonian fluid that cannot be compressed. The equation for calculating the viscosity of Newtonian fluid was given as follows:

$$\text{viscosity} = \frac{TS}{S}, \quad (2)$$

In equation (2), TS was the shear stress, and S referred to the shear rate.

However, a large number of studies had confirmed that most fluids were non-Newtonian fluids, and materials can change with the change of shear rate or time [12]. Therefore, the viscosity value of blood would not be constant. If the simulated fluid of blood was set to viscoelastic body, the calculation complexity and the amount of calculation would be greatly increased. Therefore, the simulated blood fluid was set to Newtonian fluid with a viscosity of $0.0035 \text{ kg}\cdot\text{ms}^{-1}$, and the density was set to 1060 kg m^{-3} in this study. Then the CFX software was adopted to simulate the full 3D steady-viscosity numerical value, and ANSYS software was adopted for dynamic analysis of the structural transient state, and the data exchange of the coupling surface was realized by the MFX-ANSYS/CFX platform. Due to the elasticity of the arterial wall, the arterial wall in the body was deformed caused by the flow of blood, and the flow of blood would also change at this time. It was necessary to use the Lagrangian-Euler method to describe the mechanical description of the transient fluid-solid coupling of blood [13].

In this study, the fluid governing equation was defined as the incompressible Navier-Stokes equation, and the analysis type was set to transient. The initial values of parameters such as fluid velocity, pressure, vessel wall displacement, and shear stress were set to zero. The inner wall of the blood vessel was set as a fluid-solid coupling surface. The cardiac cycle was set to 1, the total cycle was 10, and the step length was set to 0.05 s. The output control was variables such as blood vessel wall pressure, speed, and blood vessel wall shear stress. The pressure value of the blood vessel entrance was set as a function of time (the pressure-time curve is shown in Figure 2(a)), and the restriction conditions were set for the entrance and exit of the blood vessel wall (as shown in Figure 2(b)), then the final pressure of the blood vessel exit was set to 50 Pa. The iterative graph (as shown in Figure 2(c)) could test the rationality of the boundary conditions. When the lines were more concentrated, it indicated that the boundary conditions were reasonable. Finally, the solution was automatically completed under the monitoring of the software.

2.3. Construction of the Balloon Model. The role of balloons in PTA was very important. Compared with nonfolded balloons, multifolded balloons had a better effect in the process of vasodilation. Therefore, a balloon structure with 6 folds and tapered ends was adopted in this study. The CAD software was adopted to construct the balloon model. The modeling process was mainly divided into four steps: parameter calculation and 1/6 sketch construction, sketch generation, balloon straight section based on curved surface stretching, and construction of the tapered end module a 1:1 ratio of length to diameter. The balloon material was defined as a membrane material, so the meshing was relatively simple. The meshing tool that came with the ABAQUS software was adopted to mesh the balloon model, and 4 nodes were selected to reduce the integral membrane element, and the size of the largest element was 0.02 mm. The balloon material was mainly thermoplastic polyester, so the Young's modulus of the material was 1455 MPa, the Poisson's ratio was 0.3, and the density was $1.26 \times 10^{-3} \text{ g mm}^{-3}$.

The complete deformation process of balloon expansion was divided into four stages: compression and contraction before implantation, bending and delivery to the lesion, balloon inflation, and rebound after balloon pressure unloading. Therefore, compression and contraction of the balloon and bending delivery were also required in the simulation of PTA.

The expansion and resilience of balloon were nonlinear problems, which mainly involved materials (elastoplasticity of metal materials), balloon and plaque materials, geometric nonlinearity (maximum deformation under external load conditions), and contact nonlinearity of the state. Therefore, the use of finite element for dynamic analysis was very suitable for solving such problems. At each moment in the above process, the system was almost in equilibrium, and the system state parameters at any time were determined by the value, so the whole process composition could be regarded as a state of close equilibrium, which was a quasi-static process. In the process of PTA simulation analysis, the maximum deformation of the balloon was the most complex nonlinear issue. Therefore, ABAQUS/Explicit quasi-static process was adopted for simulation analysis and solution. The friction coefficient of the penalty function was set to 0.2, the contact simulation was self-contact, the expansion time was 1 ms, and the rebound time was 0.5 ms. In addition, the vascular lumen would increase after a specific pressure was applied to the balloon; and after the pressure was unloaded, the blood vessel would rebound linearly to varying degrees.

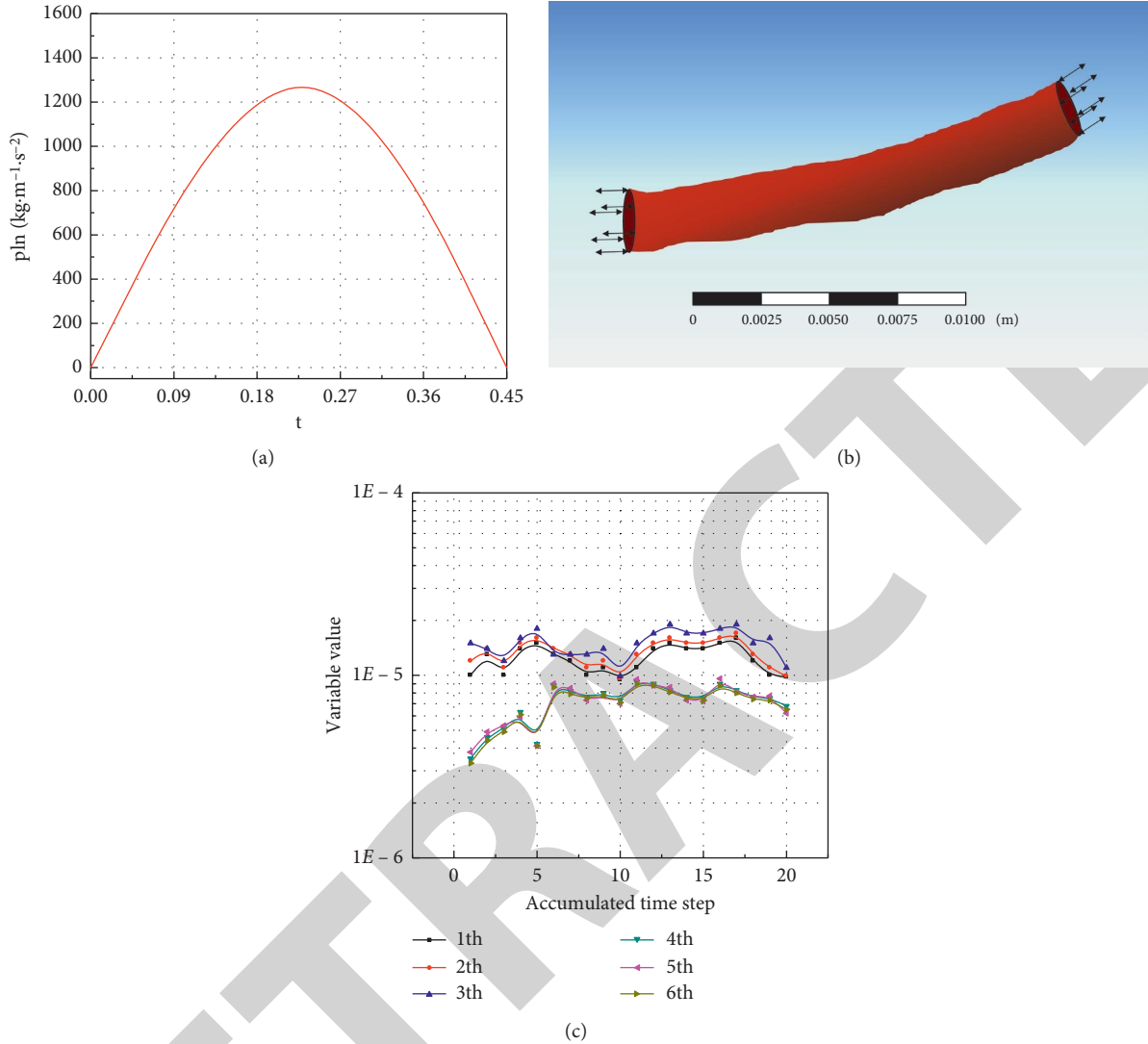


FIGURE 2: Setting of related parameters: (a) vessel inlet pressure-time curve; (b) vessel wall inlet and outlet restriction setting; (c) iterative diagram.

Therefore, the applied pressure value on the inner surface of the balloon could be set to 1.2 MPa, and drawing the smoothing step amplitude curve could gradually reduce the load to 0.01 MPa. The centerline of the blood vessel after rebound was extracted for subsequent analysis, and the vascular dynamic effect caused by the movement of the structure of the viscous pressure was introduced (balloon expansion and vascular wall shock during rebound). The calculation equation of viscous pressure was given as follows:

$$\begin{aligned}
 C_v &= -\rho \cdot C_d, \\
 &= -\rho^2 \sqrt{\left(\frac{E}{\rho}\right)}. \quad (3)
 \end{aligned}$$

In equation (3), C_d was the propagation velocity, E is referred to the Young's modulus (0.3 MPa), and ρ represented the density ($1.12 \times 10^{-3} \text{ g mm}^{-3}$). The calculated viscous pressure C_d was about $-0.25 \times 10^{-3} \text{ MPa}$.

2.4. Experimental Animal and Model Construction.

Twenty healthy New Zealand white rabbits were taken as the research objects (no limited to males and females), with a weight range of 2.5~3.0 kg and an age of 3~4 months old. The experimental animals were provided by the XX. All animals were fed with ordinary feed, and the experimental operations were in accordance with the principles of animal experiment ethics. All experimental rabbits were reared in a single cage and bred adaptively for 14 days at a room temperature of 27 C, free drinking water, and ordinary feed.

The rabbits were weighed before surgery, and injected with 0.5 mg kg^{-1} 3% pentobarbital sodium along the ear vein for anesthesia treatment. They were fixed on the animal operating table at a supine position, and then performed with the tracheal intubation and detection of basal blood lipid level. The venous access was opened from the ear vein, and the access was maintained by continuous injection of glucose and sodium chloride injection. The skin was prepared on the left groin area, shaved, and sterilized with

iodophor, an incision about 5.0 cm in length was made to bluntly separate the skin, subcutaneous tissue, and muscle before exposing and freeing the femoral artery. The blood flow was ligated and blocked at the distal and proximal ends of the femoral artery; the blood vessel was punctured with a needle and insert a 0.018 guide wire to insert the balloon (3.5 mm diameter) about 20 cm. After the guide wire was taken out, it was injected with normal saline, and the pressure was maintained at 12 atm. The balloon was taken back to the iliac artery, the balloon was withdrawn, the negative pressure was maintained, and then the balloon was returned to the original place. The above steps were repeated for 4 times. The artery was ligated after the balloon was removed, and the incision was sutured. After the surgery, the incision was cleaned with iodophor, and the test rabbit was put to the rabbit cage again. When the rabbit wakened up naturally, it was injected intramuscularly with 800,000 units of penicillin for continuous 3 days, and finally fed with high-fat feed (84% ordinary feed + 5% lard + 1% cholesterol + 10% egg yolk powder) for continuous 3 months.

2.5. Grouping. The experimental rabbits were randomly divided into a conventional PTA group and a VR-PTA group. All test rabbits were weighed before surgery and were anesthetized with 0.5 mg/kg 3% pentobarbital sodium injected along the ear vein.

The rabbits in the PTA group were shaved off the left inner thigh and abdomen hair. After disinfection with iodophor, an incision was made about 4 cm longitudinally along the femoral artery. The skin, subcutaneous tissue, and muscle were bluntly separated, and the femoral artery was exposed and freed. Step 1.4 was repeated for balloon expansion treatment, and each expansion time was 30 s, which were repeated for 4 times. Then, the balloon was withdrawn, and the routine suture, disinfection, and anti-infection treatment were performed.

The experimental rabbits in the VR-PTA group all were performed with the balloon expansion of virtual PTA using the ABAQUS/Explicit software, and the quasi-static analysis mode was adopted. The simulation process was mainly balloon expansion, which was divided into two stages: expansion (1 ms) and rebound (0.5 ms). A pressure of 34.3 KPa was applied to the inner surface of the balloon, 7.14 Pa viscous pressure was applied to the outer surface of the blood vessel wall, and the kinetic energy/internal energy ratio had to be less than 5% so as to suppress the dynamic oscillation of the blood vessel. The four typical time points had to be paid attention: before the simulation (T1), after the balloon was inserted (T2), the maximum balloon expansion time (T3), and the end of vascular rebound (T4). The maximum stress was selected as the evaluation variable of the stress distribution, that was, the circumferential tension caused by balloon expansion on the vessel wall. PTA treatment was performed after the simulation was completed. The operation steps of the surgery were the same as those in the PTA group but had to be adjusted in time according to the results of the operation simulation.

2.6. Measurement Indicators. The experimental animals were sacrificed at the 7th, 14th, and 28th day after the surgery, and the blood vessel specimens of the lower extremities were collected. The Image-Pro-Plus software was used to measure the vascular lumen cross-sectional area, vascular wall thickness, vascular intima area, vascular media area, and vascular adventitia area. In addition, the intima/media area ratio (I/M) and Lumen/Tube wall adventitia area ratio (LA/TA) were calculated.

2.7. Statistical Analysis of Experimental Data. The experimental data were processed and analyzed using the SPSS 22.0 software. The measurement data were expressed as mean \pm standard deviation, and the difference was compared with independent sample *t*-test. $P < 0.05$ indicated that the difference was statistically significant.

3. Results and Analysis

3.1. 3D Model of LEAO and Vascular Hydrodynamic Analysis. A 3D model of normal arteries and stenotic arteries was constructed in this study (as shown in Figure 3). It showed that compared with the normal arterial blood vessel and blood model, the stenotic arteries and blood vessels showed obvious “torsion,” and the blood was consistent with the “torsion” of the stenotic vessels. Therefore, “twisting” arteries were adopted in this study to simulate the stenosis of blood vessels.

Then, the pressures of the blood vessel wall pressure at different blood vessel observation points were compared (as shown in Figure 4). Figure 4(a) illustrates that the pressure changes at the three observation points of normal blood vessels basically conformed to the law of gradual decrease from input to outlet. The difference between observation point 2 and observation point 3 was small, and both were much smaller than that in the observation point 1. Figure 4(b) illustrates that the pressure at the observation point 2 of the stenotic blood vessel was the smallest, which was a negative value. At the same time, the difference of it to the observation points 1 and 3 gradually increased. Such results indicated that the blood reflux may occur in the stenosis of the blood vessel, and the change of hemodynamic parameters was greatly reduced, which was in line with the clinical physical law [14–16].

Next, the distribution of shear stress on the vessel wall was analyzed (as shown in Figure 5). Shear stress referred to the interaction internal force generated by various parts of the object when the object was deformed by external influence factors (such as pressure, humidity, and temperature field changes). The force component along the tangential direction was called shear stress. Figure 5(a) discloses that the gradient of the shear stress distribution of normal blood vessels was small. The peak value at observation point 2 was about 29.8 Pa, while the peak values at observation point 1 and observation point 3 were 15.6 Pa and 11.2 Pa, respectively. The difference was relatively small. Figure 5(b) reveals that the peak value at observation point 2 of the stenotic blood vessel was about 55.6 Pa, while the peak values at

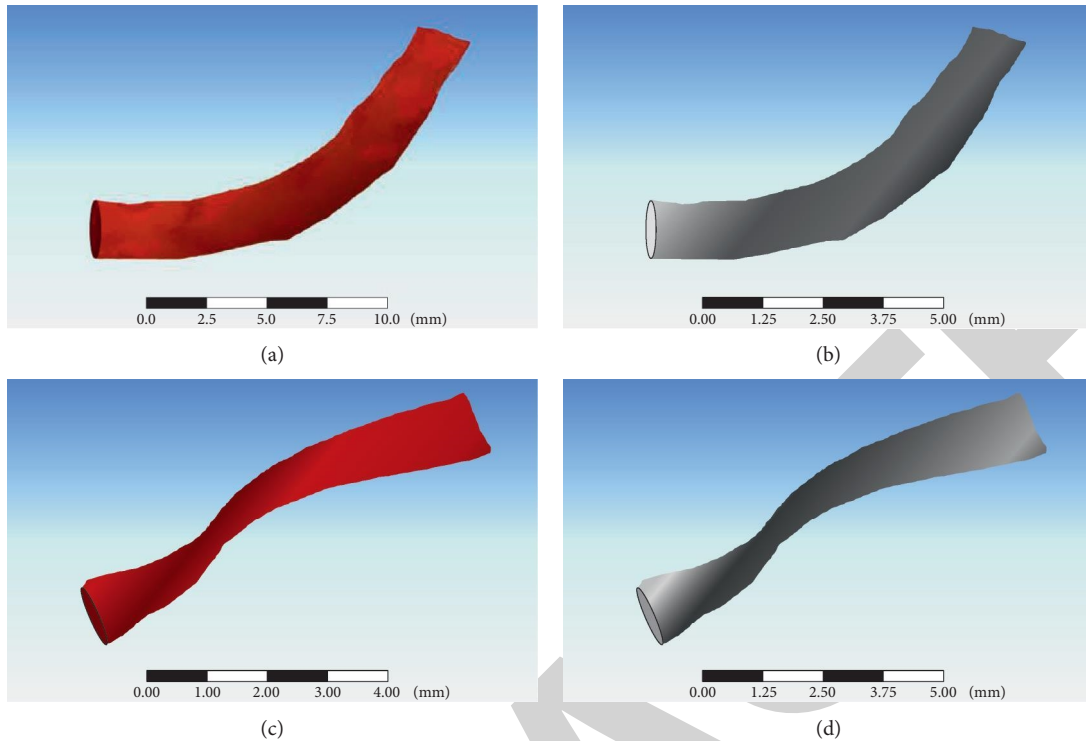


FIGURE 3: Blood and blood vessel model of arterial stenosis: (a) normal arterial blood model; (b) normal arterial blood vessel model; (c) stenotic arterial blood model; (d) stenotic arterial blood model.

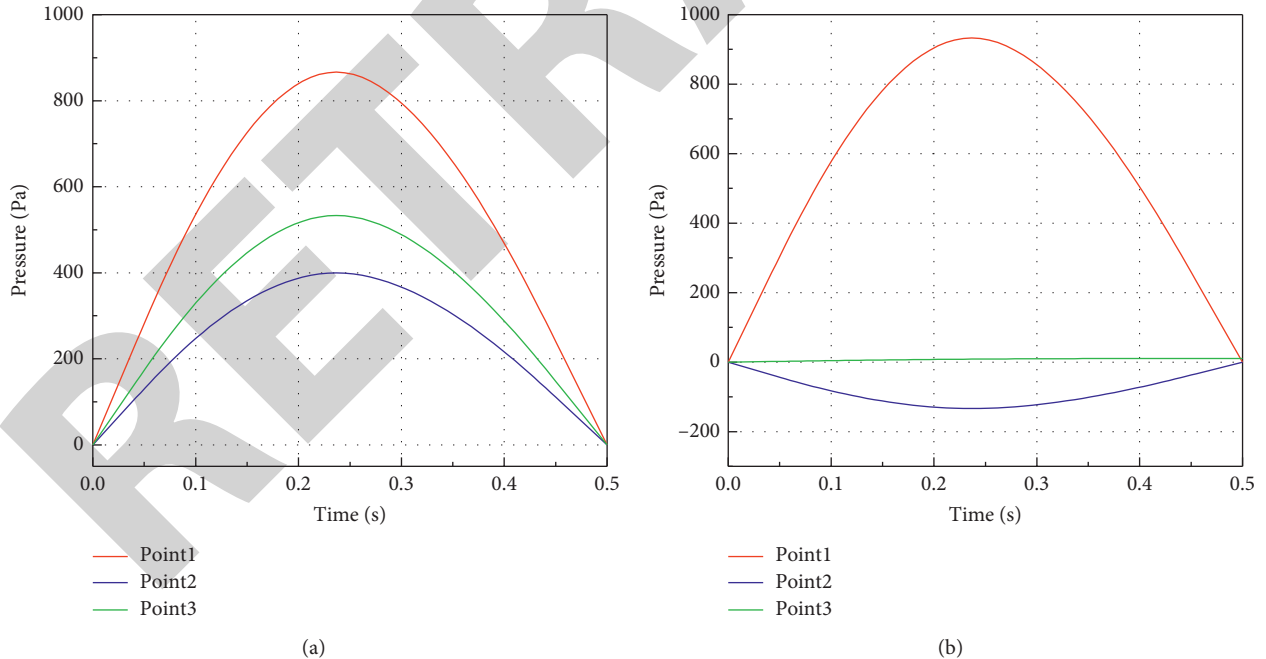


FIGURE 4: The pressures of the blood vessel wall pressure at different blood vessel observation points: (a) pressure change at each observation point of the normal arterial vessel model; (b) pressure change at each observation point of the stenotic arterial vessel model.

observation points 1 and 3 were 10.1 Pa and 2.3 Pa, respectively, and the difference was relatively large. It showed that the shear stress distribution of stenotic blood vessels could gradually increase with the stenosis of the blood vessels [17].

3.2. Verification on the Simulation Process of Balloon Expansion. The balloon expansion process was simulated using ABAQUS/Explicit module, and the quasi-static analysis was performed with a stable general contact algorithm. In the calculation process, some measures were

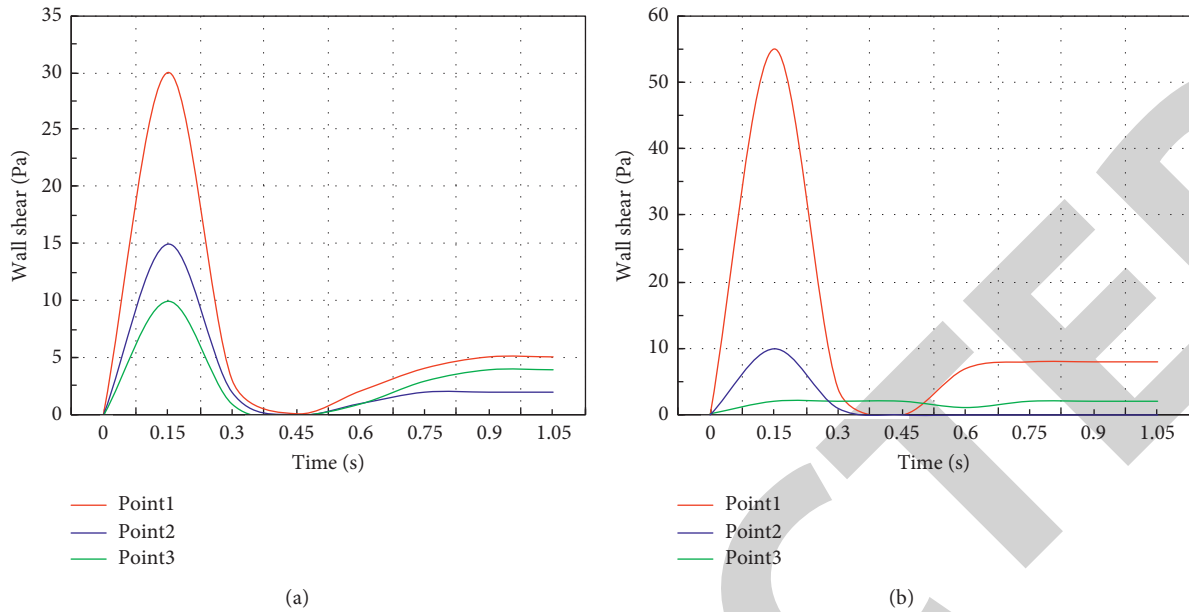


FIGURE 5: Comparison of blood vessel shear stress between normal and sclerotic arteries: (a) change of shear stress at each observation point of the normal arterial vessel model; (b) change of shear stress at each observation point of the stenotic arterial vessel model.

adopted to save the calculation cost, such as increasing the load rate and semiautomatic mass scaling to speed up the solution, ensuring that the ratio of kinetic energy/internal energy during simulation was not higher than 5%. Figure 6 illustrates that the energy ratio peak was found at about 0.0001 s from the beginning of the balloon expansion simulation. It showed that under the early initial boundary conditions, the applied load could cause violent contact between the balloon and the vessel wall in a short time. Then, the energy ratio immediately decreased to below 5%, indicating that the kinetic energy ratio of the model was very low, and the contact inertia effect would hardly affect the final analysis result, so the previous peak effect could be ignored.

The impacts of balloon expansion on the diameter of the lumen, cross-sectional area, circumferential distance, and cross-sectional diameter of the proximal 5 mm, balloon dilated, and distal 5 mm of the stenotic vessel were analyzed in this study. Figure 7 reveals that after balloon expansion, the improvement of the vascular lumen diameter in the stenosis was the most obvious, and the balloon expansion caused by the internal pressure load and the linear rebound produced by the vasoconstriction force were the main factors affecting the diameter of the lumen. Figure 7(a) discloses that there was about 15 mm vascular lumen diameter was below 1.5 mm, about 6 mm vascular lumen diameter was below 1.0 mm, and the smallest diameter was only 0.77 mm. Figure 7(b) suggests that the minimum blood vessel cross-sectional area was 0.6 mm^2 at the beginning. Figure 7(c) indicates that the minimum section circumferential distance was 2.3 mm at the beginning. Therefore, there was a more serious lesion feature.

In the PTA process, the diameter data at different times and at different cross-sectional positions are shown in

Figure 7(d). Parts A, B, and C in Figure 7(d) reveal that the average diameter increase ratio of the proximal 5 mm section at T1 was about 14%, the average diameter increase ratio of the balloon at T1 was about 3%, and the increase ratio of the average cross-sectional diameter of the distal 5 mm at T1 was about 14%, indicating that balloon expansion could obviously increase the diameter of the vascular lumen. At T3, the average vascular lumen diameter rebounded by about -15% after the balloon expansion was completed, and the lumen at the narrowest part rebounded by about 20%. It showed that the distal 5 mm blood vessel segment was larger than the proximal 5 mm blood vessel segment, which may be caused by the reference diameter of the proximal blood vessel being larger than the distal blood vessel.

3.3. The Effect of VR-Assisted PTA on the Stenosis of Blood Vessels in Experimental Rabbits. PTA had the most obvious effect on improving the diameter of stenotic vessels [18]. The effect of virtual PTA on the vascular lumen of experimental rabbits in the VR-PTA group was analyzed (as shown in Figure 8). It indicated that the average diameter of the proximal 3 mm vascular lumen of the expanded segment at T1 and T2 increased by about 40%, the average diameter of the proximal 5 mm nonexpanded vascular lumen increased by about 18%, and the distal expanded and nonexpanded vascular lumen increased by about 18%. The average diameter increased by about 25% and 10%, respectively. Compared with the diameter at T2, the diameter of the expanded vascular lumen at T3 was reduced by 21% and 13%, and the distribution was uniform; the rebound rate of proximal and distal vascular lumen was about -10% and -15% , respectively. It showed that balloon expansion could improve the lumen diameter of narrowed blood vessels to a

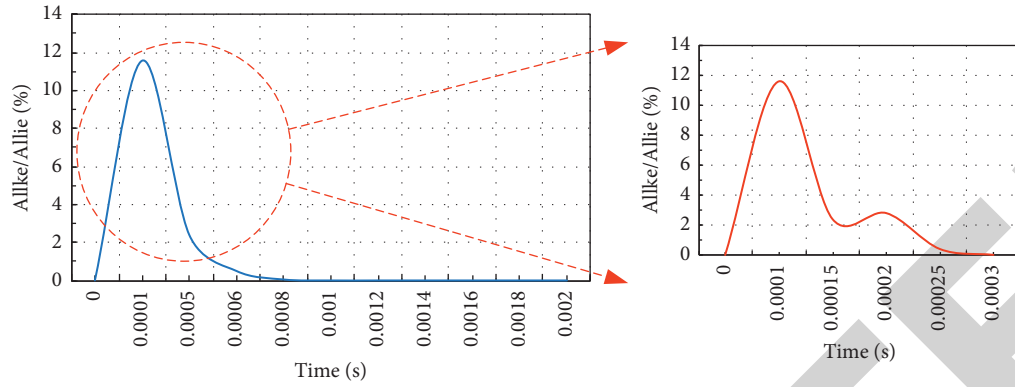


FIGURE 6: Diagram of the kinetic energy/internal energy ratio of balloon expansion.

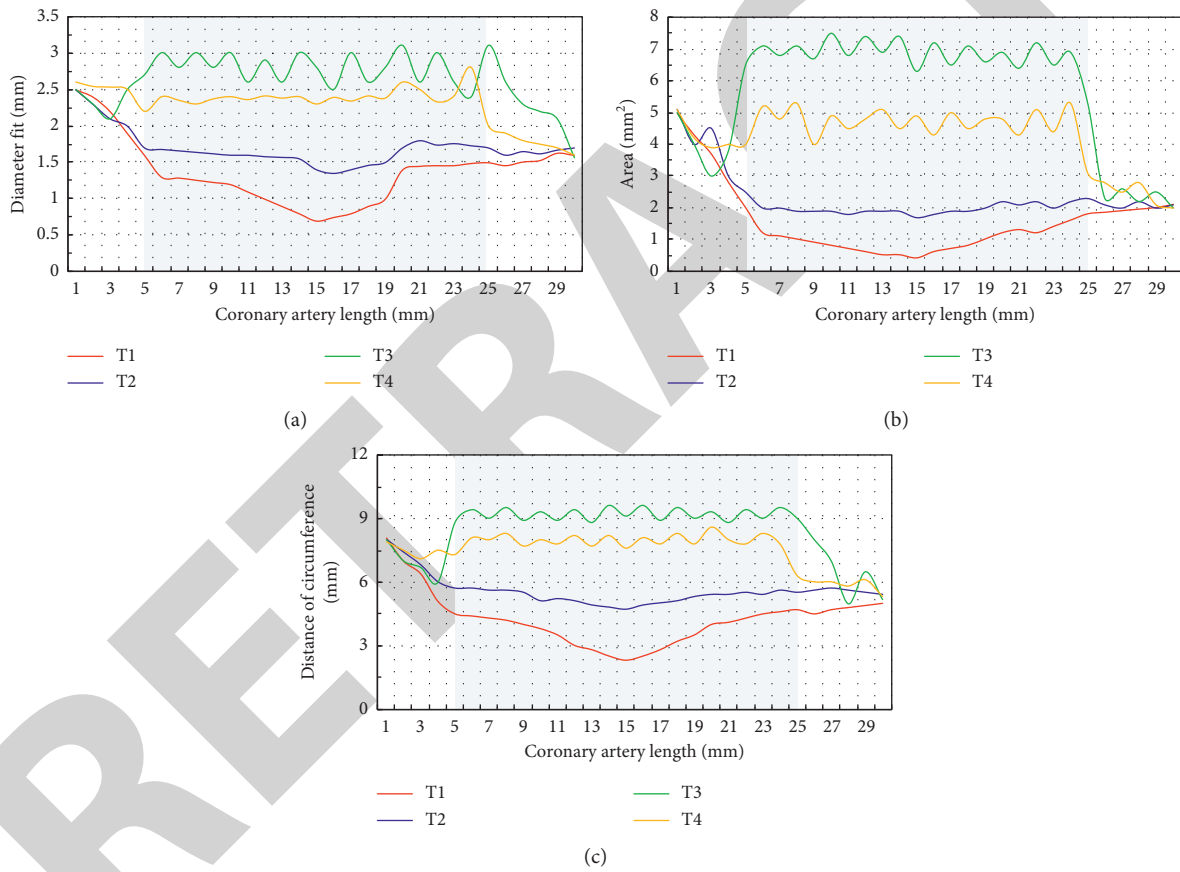


FIGURE 7: Continued.

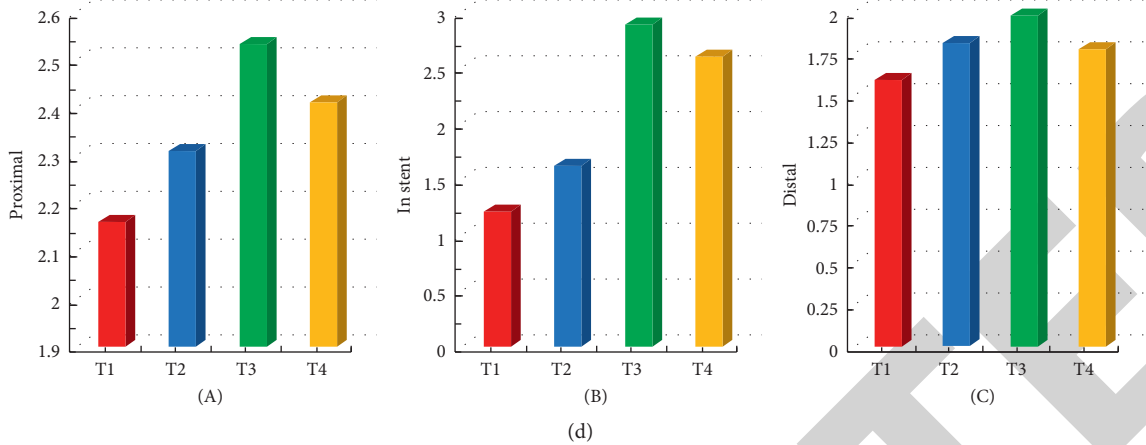


FIGURE 7: Changes on related parameters of vascular lumen at different times during PTA: (a) changes of vascular lumen diameter; (b) changes of vascular lumen cross-sectional area; (c) cross-sectional circumferential distance of vascular lumen; (d) cross-sectional diameter of vascular lumen (A shows the diameter at proximal 5 mm, B shows the diameter of balloon angioplasty, and C shows the diameter at distal 5 mm); and the gray areas (a–c) represent the time of balloon angioplasty.

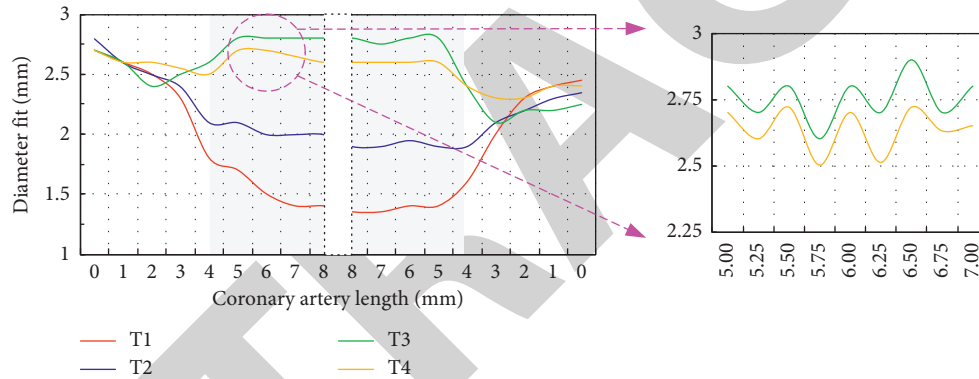


FIGURE 8: Diameter changes of vascular lumen in the expanded and nonexpanded segments.

certain extent [19]. However, the diameter of the vascular lumen after expansion was slightly smaller than the standard diameter of the expansion balloons due to the rebound effect of blood vessels.

The impacts of virtual PTA on the ellipticity of the cross-sectional area of the marginal vascular lumen were analyzed (as shown in Figure 9). It revealed that the ellipticity of the cross-sectional area of the stenotic vessel at T1 was higher than that of the nonexpanded vascular lumen; it gradually decreased to the level of the nonexpanded blood vessel at T2, indicating that balloon expansion could play a certain plastic effect of vascular lumen; that at T3 gradually stabilized; and that at T4 gradually decreased, and the ellipticity of the cross-sectional area of the expanded and nonexpanded vascular lumen has hardly changed.

During the PTA surgery, the geometry of blood vessels would undergo stress changes with the expansion of the balloon and pressure unloading. Therefore, the stress state could feed back the mechanical properties of blood vessels, which could then be undertaken as indicators for evaluating vascular damage [20, 21]. For this reason, the impacts

of virtual PTA on the internal stress distribution of marginal blood vessels were analyzed (as shown in Figure 10). Figure 10(a) shows that if the maximum principal stress value at T1 was assumed to be 0, the blood vessel would undergo changes such as expansion and rebound due to the expansion of the balloon at T2, so only a low level of stress remains inside the blood vessel. Therefore, the internal stress distribution of the expanded and nonexpanded blood vessels had changed obviously. At T3, the maximum principal stress at the proximal end could reach 0.71 MPa as the balloon expands to the maximum, the maximum principal stress at the distal end could reach 0.35 MPa, and that increased greatly. At T4, after the balloon was withdrawn, the maximum principal stress inside the blood vessel was observably reduced due to the rebound effect of the blood vessel (the dilated blood vessel was the most obvious).

Then, the change trend of stress (UL) along the long axis of the blood vessel was defined, and a variable UL was defined to evaluate the stress change. The calculation equation of the variable UL was given as follows:

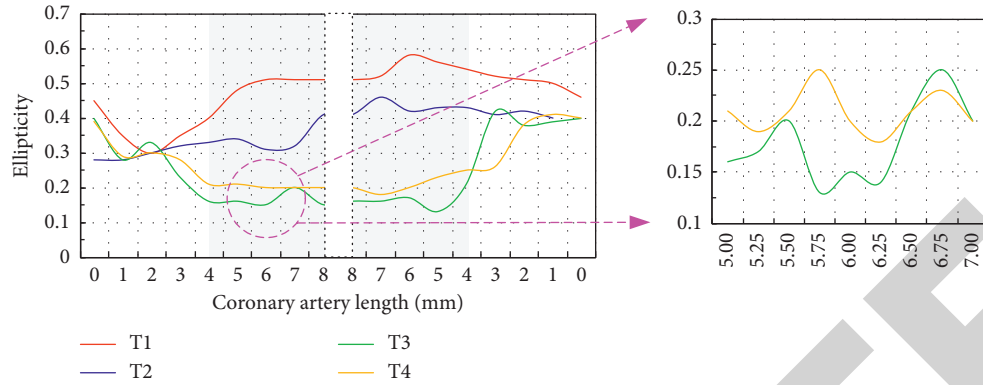


FIGURE 9: Changes in the ellipticity of the cross-sectional area of the expanded and nonexpanded vascular lumen.



FIGURE 10: Changes in the distribution of the maximum principal stress of the expanded and nonexpanded vessels: (a) the distribution change of the maximum principal stress of the blood vessel; (b) the change of the vascular variable UL.

$$U_L = \left(\frac{L_{MPS}}{U_{MPS}} \right) \cdot 100\%, \quad (4)$$

In equation (4), L was the vessel length, MPS referred to the maximum principal stress, and U represented the stent edge artery length.

Figure 10(b) illustrates that when U was about 12.8% and 8.2% of the proximal and distal blood vessels at T3, the values at T4 were about 5.3% and 8.6%, so the average value was 8.3%. It indicated that the maximum principal stress value at 3 mm of the marginal vessel was much lower than the maximum principal stress value at 5 mm (about 10% lower), so the change of maximum principal stress was the most obvious within 2 mm of balloon-expanded vessel.

3.4. Effects of VR-Assisted PTA in the Treatment of LEAO. An animal model of LEAO was constructed, and the conventional PTA and VR-assisted PTA treatment were performed. The morphological changes of the target blood vessel were evaluated at the 7th, 14th, and 28th day after

surgery (as shown in Figure 11). Figure 11(a) discloses that compared with the PTA group, the vascular lumen area of the VR-PTA group was greatly increased at all the time points after surgery ($P < 0.05$). Figure 11(b) reveals that in contrast to the PTA group, the thickness of the vessel wall in the VR-PTA group was observably reduced at the 7th and 28th day after the surgery ($P < 0.05$). Figure 11(c) illustrates that the intimal area of the VR-PTA group increased dramatically at the 14th day after surgery in contrast to the PTA group ($P < 0.05$), but the intimal area decreased remarkably at the 28th day after surgery ($P < 0.05$). Figure 11(d) indicates that the vascular media area of the VR-PTA group was reduced greatly than that in the PTA group at the 14th and 28th day after the surgery ($P < 0.05$). Figure 11(e) suggests that the I/M of the VR-PTA group increased much in contrast to the PTA group at the 7th day after the surgery ($P < 0.05$), but the I/M at the 14th and 28th day after surgery was reduced dramatically ($P < 0.05$). Figure 11(f) suggests that compared with the PTA group, the ratio of vascular lumen to adventitia of the VR-PTA group increased dramatically at the 7th and 28th day after the surgery ($P < 0.05$).

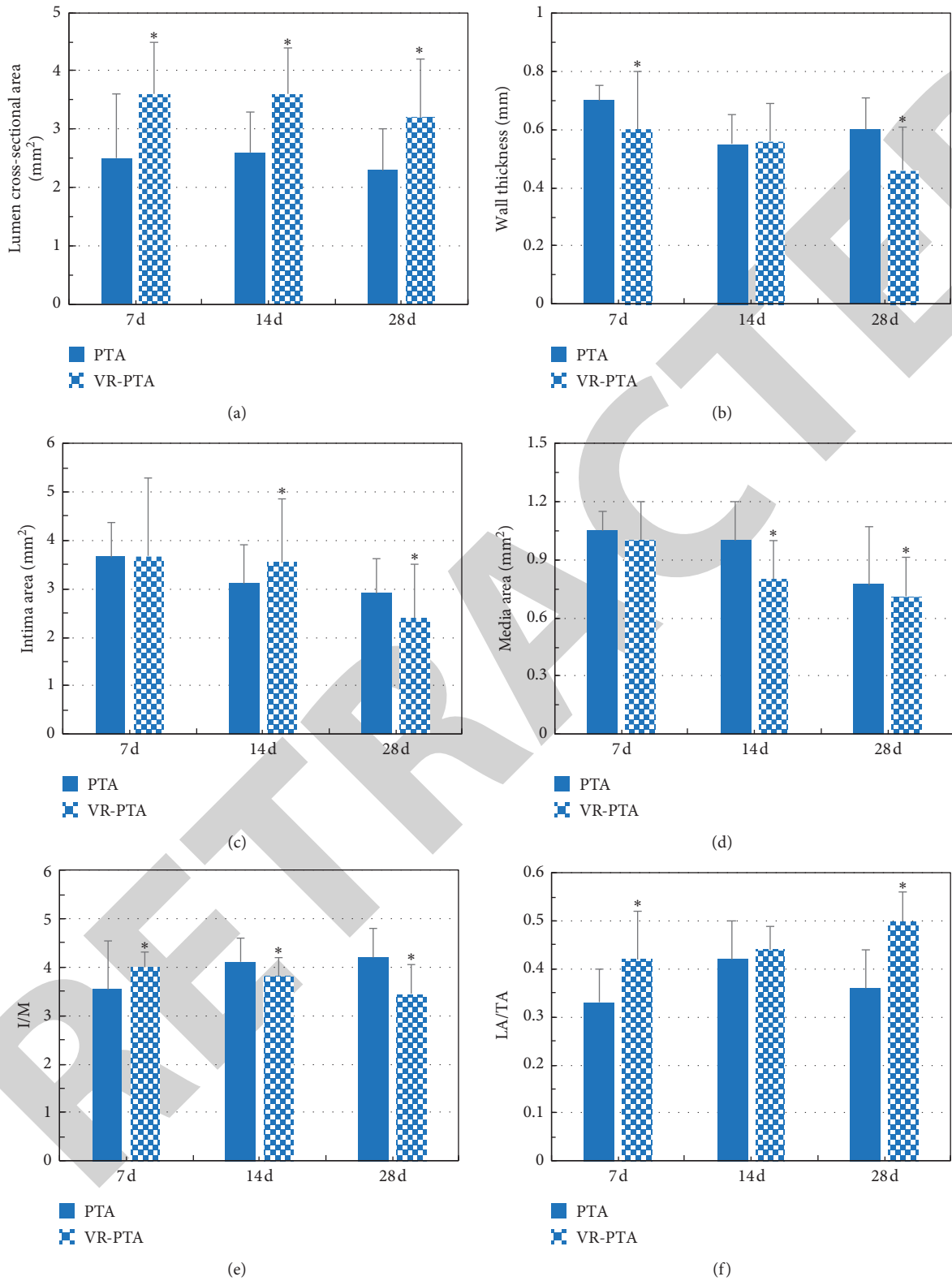


FIGURE 11: Comparison of vascular lumen-related parameters of animal models of lower-extremity arteriosclerosis in different groups: (a) cross-sectional area of vascular lumen; (b) thickness of vascular wall; (c) vascular intima area; (d) vascular media area; (e) I/M; (f) vascular lumen/vascular adventitia area. The symbol * indicates that the difference was statistically different in contrast to PTA group ($P < 0.05$).

4. Conclusion

In this study, the virtual implantation simulation analysis of PTA was performed to evaluate the morphology and stress distribution changes of blood vessels during the treatment process. The results found that the initial plasticity of the stenosis lumen could be achieved after balloon expansion, and the diameter and area of the stenosis vascular lumen could be changed, which provided the foundation for the subsequent application of animal experiments. The virtual implantation simulation treatment of LEAO animal model PTA was realized. Compared with conventional PTA, the VR-PTA could increase the lumen area and reduce the intima and media areas. However, it only analyzed the therapeutic effect of VR-PTA in an animal model and did not combine the analysis of changes in blood flow and fluid mechanics and failed to consider the initial stress state of the blood vessel in this study. In the follow-up, it is necessary to use clinical patient image data to conduct the analysis of the curative effect of the virtual simulation-assisted PTA, while considering the simulation and verification of complex lesions. In short, the results of this study could provide reference for improving the therapeutic effect of LEAO.

Data Availability

The data used to support the findings of this study are available from the corresponding author upon request.

Conflicts of Interest

The authors declare no conflicts of interest.

Acknowledgments

This work was supported by the Fundamental Research Funds for the Central Universities (0214-14380481), and the Project funded by China Postdoctoral Science Foundation (2020M670035ZX), and the Natural Science Foundation of Jiangsu Province (SBK2020040321), and the Postdoctoral Research Funding Program of Jiangsu Province (2020Z368), and the 2020 Jiangsu Province Shuangchuang Ph.D. Introducing Talent Project of Nan Hu.

References

- [1] J. M. Firnhaber and C. S. Powell, "Lower extremity peripheral artery disease: diagnosis and treatment," *American Family Physician*, vol. 99, no. 6, pp. 362–369, 2019.
- [2] Society for Vascular Surgery Lower Extremity Guidelines Writing Group, M. S. Conte, F. B. Pomposelli, and D. G. Clair, "Society for Vascular Surgery practice guidelines for atherosclerotic occlusive disease of the lower extremities: management of asymptomatic disease and claudication," *Journal of Vascular Surgery*, vol. 61, pp. 2S–41S, 2015.
- [3] Y. Zhu, X. Xian, and Z. Wang, "Research progress on the relationship between atherosclerosis and inflammation," *Biomolecules*, vol. 8, no. 3, p. 80, 2018.
- [4] X. Li, X. Liu, X. Li, L. Xu, X. Chen, and F. Liang, "Tortuosity of the superficial femoral artery and its influence on blood flow patterns and risk of atherosclerosis," *Biomechanics and Modeling in Mechanobiology*, vol. 18, no. 4, pp. 883–896, 2019.
- [5] B. Li, X. Lu, M. Moeini, S. Sakadžić, E. Thorin, and F. Lesage, "Atherosclerosis is associated with a decrease in cerebral microvascular blood flow and tissue oxygenation," *PLoS One*, vol. 14, no. 8, Article ID e0221547, 2019.
- [6] E. Jahic, H. Avdagic, I. Iveljic, and A. Krdzalic, "Percutaneous transluminal angioplasty of subclavian artery lesions," *Medical Archives*, vol. 73, no. 1, pp. 28–31, 2019.
- [7] K. Ejiri, A. Ogawa, S. Fujii, H. Ito, and H. Matsubara, "Vascular injury is a major cause of lung injury after balloon pulmonary angioplasty in patients with chronic thromboembolic pulmonary hypertension," *Circulation Cardiovascular Interventions*, vol. 11, no. 12, Article ID e005884, 2018.
- [8] S. M. Imani, A. M. Goudarzi, S. E. Ghasemi, A. Kalani, and J. Mahdinejad, "Analysis of the stent expansion in a stenosed artery using finite element method: application to stent versus stent study," *Proceedings - Institution of Mechanical Engineers H*, vol. 228, no. 10, pp. 996–1004, 2014.
- [9] G. S. Karanasiou, C. Conway, and M. I. Papafaklis, "Finite element analysis of stent implantation in a three-dimensional reconstructed arterial segment," in *Proceedings of the Annual International Conference IEEE Engineering in Medicine Biology Society*, pp. 5623–5626, Chicago, Illinois, August 2014.
- [10] R. Yoshida, H. Ishii, and I. Morishima, "Impact of adjunctive use of guide extension catheter on midterm outcome of drug-coated balloon angioplasty," *EuroIntervention*, vol. 15, no. 8, pp. 688–691, 2019.
- [11] G. A. Holzapfel, G. Sommer, C. T. Gasser, and P. Regitnig, "Determination of layer-specific mechanical properties of human coronary arteries with nonatherosclerotic intimal thickening and related constitutive modeling," *American Journal of Physiology-Heart and Circulatory Physiology*, vol. 289, no. 5, pp. H2048–H2058, 2005.
- [12] G. Nava, T. Yang, and V. Vitali, "Newtonian to non-Newtonian fluid transition of a model transient network," *Soft Matter*, vol. 14, no. 17, pp. 3288–3295, 2018.
- [13] D. M. Espino, D. E. T. Shepherd, and D. W. L. Hukins, "Evaluation of a transient, simultaneous, arbitrary Lagrange-Euler based multi-physics method for simulating the mitral heart valve," *Computer Methods in Biomechanics and Biomedical Engineering*, vol. 17, no. 4, pp. 450–458, 2014.
- [14] R. W. Arhart, "A possible haemodynamic mechanism for amyotrophic lateral sclerosis," *Medical Hypotheses*, vol. 75, no. 4, pp. 341–346, 2010.
- [15] M. V. Caruso, S. De Rosa, C. Indolfi, and G. Fragomeni, "Computational analysis of stenosis geometry effects on right coronary hemodynamics," in *Proceedings of the Annual International Conference IEEE Engineering in Medicine Biology Society*, pp. 981–984, Chicago, Illinois, August 2015.
- [16] C. Yuhn, K. Hoshina, K. Miyahara, and M. Oshima, "Computational simulation of flow-induced arterial remodeling of the pancreaticoduodenal arcade associated with celiac artery stenosis," *Journal of Biomechanics*, vol. 92, pp. 146–154, 2019.
- [17] Y. Shan, J. Li, and Y. Wang, "Aortic shear stress in patients with bicuspid aortic valve with stenosis and insufficiency," *The Journal of Thoracic and Cardiovascular Surgery*, vol. 153, no. 6, pp. 1263–1272, 2017.
- [18] W. E. Kok, R. J. Peters, and G. Pasterkamp, "Early lumen diameter loss after percutaneous transluminal coronary angioplasty is related to coronary plaque burden: a role for viscous plaque properties in early lumen diameter loss," *The*

- International Journal of Cardiovascular Imaging*, vol. 17, no. 2, pp. 111–121, 2001.
- [19] Y. Kuserli and A. A. Kavala, “Retrograde popliteal access and balloon dilatation of chronic total occlusion of superficial femoral arteries,” *Annals of Vascular Surgery*, vol. 64, pp. 253–262, 2020.
- [20] N. Li, F. Mendoza, and S. Rugonyi, “Venous biomechanics of angioplasty and stent placement: implications of the poisson effect,” *Journal of Vascular and Interventional Radiology*, vol. 31, no. 8, pp. 1348–1356, 2020.
- [21] A. Daoudal, J. Gindre, and F. Lally, “Use of numerical simulation to predict iliac complications during placement of an aortic stent graft,” *Annals of Vascular Surgery*, vol. 61, pp. 291–298, 2019.

RETRACTED